Decolorization of C.I. Reactive Red 2 by UV/TiO$_2$/PAC and visible light/TiO$_2$/PAC systems

Chao-Yin Kuo[a], Chung-Hsin Wu[b,*], Shih-Ting Chen[b]

[a]*Department of Safety Health and Environmental Engineering, National Yunlin University of Science and Technology, Yunlin, Taiwan*
[b]*Department of Chemical and Materials Engineering, National Kaohsiung University of Applied Sciences, 415 Chien Kung Road, Kaohsiung, Taiwan*
Email: wuch@kuas.edu.tw

ABSTRACT

In this work, the sol-gel method is utilized to synthesize TiO$_2$/powder-activated carbon (PAC) from TiCl$_4$ and PAC. The TiO$_2$/PAC system was used to decolorize C.I. Reactive Red 2 (RR2) under ultraviolet (UV) and visible light irradiation. The surface characteristics of TiO$_2$ and TiO$_2$/PAC were analyzed by X-ray diffractometer, scanning electron microscopy, transmission electron microscopy, UV-vis spectroscopy, BET surface area analysis, and X-ray photoelectron spectroscopy (XPS). The effects of the C/Ti ratio, calcination temperature, photocatalyst dose, RR2 concentration, wavelength of light, and pH on the decolorization of RR2 by TiO$_2$/PAC were evaluated. The optimal calcination temperature for forming TiO$_2$ and TiO$_2$/PAC was 400°C; moreover, the surface areas of TiO$_2$ and TiO$_2$/PAC were 42 and 108 m^2/g, respectively. The sizes of the aggregates of TiO$_2$ and TiO$_2$/PAC particles were approximately 40 and 30 nm, respectively. Experimental results reveal that the percentage of anatase increased with the amount of PAC in TiO$_2$/PAC. The spectra indicate that C doping of TiO$_2$ shifted the absorption edge from 418 nm to a longer wavelength of 471 nm. XPS characterization verifies the substitution of the C species in the crystal lattice in TiO$_2$/PAC for O species, forming Ti–O–C. As the C/Ti ratio and the TiO$_2$/PAC dosage increased, the decolorization efficiency increased. Conversely, the decolorization rate decreased as the RR2 concentration and pH increased. The TiO$_2$/PAC was photoexcited by irradiation by UV and visible light; however, TiO$_2$ was photoexcited only by UV irradiation. The efficiency of TiO$_2$/PAC was better than that of TiO$_2$ in both decolorization and total organic carbon removal.

Keywords: TiO$_2$; Powder-activated carbon; Decolorization; Photocatalytic

1. Introduction

Dyes are important water pollutants that are typically present in effluents from textile, leather, paper, and dye manufacturing. The toxicity of several dyes makes them environmentally hazardous. Small amounts of dyes can be visible and adversely affect the quality of water in an environment. Accordingly, C.I. Reactive Red 2 (RR2), which is an azo dye with

the most commonly used anchor—the dichlorotriazine group—was selected as the parent compound in this study.

Among various photocatalysts, TiO_2 has attracted considerable attention because of its chemical and biological stability and high photocatalytic activity. As is well known, valence holes are photogenerated when TiO_2 particles are irradiated by ultraviolet (UV) light, resulting in the oxidation of OH^- or H_2O by holes and the formation of hydroxyl radicals that can destroy most organic compounds [1]. Oxygen acts efficiently as an electron trap, preventing recombination of photogenerated electrons and holes. Numerous investigations have proven that UV/TiO_2 is an effective method for degrading organic compounds [1–4].

In the UV/TiO_2 system, rapid unfavorable recombination of photogenerated electrons and holes in TiO_2 markedly reduces photocatalytic efficiency. Moreover, TiO_2 can only be photoexcited by UV light so photocatalysts that use only visible light are needed. Many studies have synthesized carbon-doped TiO_2 [5,6], which extends the spectral response of TiO_2 into the visible light region, improving its photocatalytic activity. Several investigations have used systems of TiO_2/activated carbon (AC) [7–13] and TiO_2/carbon nanotubes (CNTs) [5,14,15] to degrade organic compounds under irradiation by UV or visible light. Wang et al. [10] prepared TiO_2/AC under different C/Ti ratios and calcination temperatures; the photocatalysts were used to degrade Chromotrope 2R under UV irradiation. Slimen et al. [13] demonstrated that TiO_2/AC has a higher degradation rate than TiO_2 or Degussa P25 under irradiation by visible light. Despite the reported synergistic effect of TiO_2 and AC, no study has simultaneously elucidated the effects of C/Ti ratio, calcination temperature, and light wavelength on the photocatalytic activity of TiO_2/AC. In this work, TiO_2 and TiO_2/powder-activated carbon (PAC) were synthesized by the sol-gel method, and the photocatalytic activity of these photocatalysts was tested under irradiation by visible light. The objectives of this study were to (1) prepare TiO_2 and TiO_2/PAC using different C/Ti ratios and calcination temperatures; (2) identify the surface characteristics of the prepared photocatalysts; (3) evaluate the effects of pH, RR2 concentration, and TiO_2/PAC dose on RR2 decolorization, and (4) compare the RR2 decolorization efficiency of prepared photocatalysts under irradiation by light with wavelengths of 254, 365, and 410 nm.

2. Materials and methods

2.1. Materials

Titanium (IV) chloride was the source of Ti (ACROS). Ethanol and PAC were purchased from the Katayama Reagent Company. Ethanol was used as a modulator in the preparation of TiO_2 and TiO_2/PAC. The parent compound, RR2, was purchased from the Sigma–Aldrich Chemical Company. The formula, molecular weight, and maximum wavelength of the light absorbed by RR2 were $C_{19}H_{10}Cl_2N_6Na_2O_7S_2$, 615 g/mol, and 538 nm, respectively. The pH of the solution was adjusted using HNO_3 or NaOH. All compounds were used as received without further purification. All solutions were prepared using deionized water (Milli-Q) and reagent-grade chemicals.

2.2. Preparation of TiO_2 and TiO_2/PAC

Fig. 1 presents the flowchart of the procedure by which TiO_2/PAC (C/Ti = 1) was prepared. Briefly, 0.1301 g PAC was mixed with 60 mL ethanol (95%). This mixture was shaken for 10 min in an ultrasonic bath (Delta, DC 400H) and then mixed with 6 mL titanium (IV) chloride. The mixture was then stirred magnetically at 250 rpm for 24 h. After gel formation, the gel was rinsed in 10 mL ethanol (99%) and the batch was dehydrated at 120°C. Dehydrated gels were ground and then calcined at 400°C for 3 h to generate TiO_2/PAC powder. The TiO_2 particles were produced by the same procedure as was utilized to prepare TiO_2/PAC, but without adding PAC.
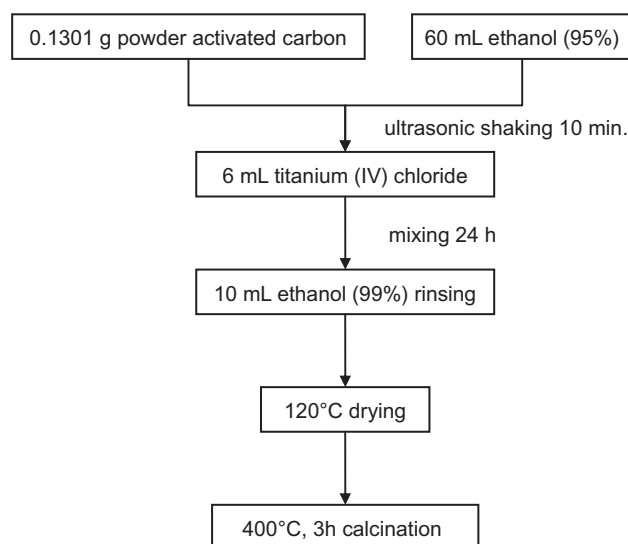
Fig. 1. Flowchart for the procedure used to prepare TiO_2/PAC (C/Ti = 0.2).

2.3. Surface characterization

The crystalline structures of the prepared TiO_2 and TiO_2/PAC were determined by X-ray diffractometer (XRD) (PANalytical X'Pert Powder). The accelerating voltage and applied current were 40 kV and 30 mA, respectively. The XRD patterns were recorded with 2θ values of 20–80°. The morphology and structure of the prepared TiO_2 and TiO_2/PAC were characterized by scanning electron microscopy (SEM) (JEOL 6330 TF) and transmission electron microscopy (TEM) (JEOL 3010). The specific surface area, pore size, and pore volume of the samples were determined using nitrogen as the adsorbate at −196°C in a static volumetric apparatus (Micromeritics ASAP 2020). UV–vis spectroscopy (Jasco V-670) was utilized to obtain the absorbance spectrum of photocatalysts at wavelengths in the range of 200–800 nm. The UV–vis diffuse reflectance spectra were used to calculate the band gap energy of the photocatalysts. The X-ray photoelectron spectroscopic (XPS) measurements were made using a vacuum generator ECSALAB MKⅡ photoelectron spectrometer (East Grinsted) with an ALKR 1, 2 (1486.6 eV) X-ray source.

2.4. Photodegradation of RR2

In all experiments, except those for determining the effect of RR2 concentration on RR2 decolorization, the RR2 concentration was 20 mg/L. The reaction pH was 7 in all runs, except in those for determining the effect of pH on RR2 decolorization. The effects of photocatalyst dosages of 0.5, 1, and 2 g/L were evaluated. Decolorization experiments were performed in a 3 L hollow cylindrical glass reactor. An 8 W lamp (254, 365, or 410 nm, Philips) was placed inside a quartz tube as the light source. The reaction temperature was 25°C in all experiments. The reaction medium was stirred continually at 300 rpm to suspend the photocatalysts. Aliquots with a total volume of 15 mL were withdrawn from the photoreactor at predetermined intervals. Suspended photocatalyst particles were separated by filtration through a 0.22 μm filter (Millipore). The RR2 concentration was measured using a spectrophotometer (Hitachi U-2001) at 538 nm. Mineralization of RR2 was identified by the reduction in total organic carbon (TOC), measured using an O.I. 1010 TOC analyzer. Some experiments were conducted in triplicate and average values were reported.

3. Results and discussion

3.1. Surface characteristics of TiO₂ and TiO₂/PAC

Fig. 2 shows the XRD patterns of TiO_2 and TiO_2/PAC. Anatase content was determined from the integrated intensity of (1 0 1) anatase diffraction, I_A, and that of (1 1 0) rutile diffraction, I_R, using Eq. (1) [16]. From these XRD patterns, the crystalline size of the prepared powders was calculated using the Scherrer formula, Eq. (2):

$$Anatase\ (\%) = \frac{1}{1 + 12.6\frac{I_A}{I_R}} \times 100 \qquad (1)$$

$$D = \frac{0.9\lambda}{\beta \cos\theta} \qquad (2)$$

where D is crystalline size in nm; λ is the X-ray wavelength (0.15418 nm); β is the line width at medium height of the anatase (1 0 1) and rutile (1 1 0) peaks, and θ is the diffraction angle [17].

The diffraction peak at $2\theta = 26.5°$ can be accurately indexed as the (0 0 2) reflection of graphite. The peaks of carbon in the pattern were not clearly recognizable due to its amorphous structure. Another likely reason is that the main peak of carbon at 26.5° overlaps the main peak of rutile TiO_2 at 27.4°. Peaks at 25.4, 37.9, 48.1, and 53.9° correspond to the diffractions of the (1 0 1), (0 0 4), (2 0 0), and (1 0 5) crystal planes of anatase, respectively (JCPDS no. 21-1272). Other crystal phases were assigned to the (1 1 0) and (1 0 1) diffraction peaks of rutile at 27.4 and 36.1°, respectively (JCPDS no. 21-1276). The XRD patterns show the diffraction peaks of a mixture of anatase and rutile, which are favorable for photocatalytic reactions [18–21]. Table 1 presents the surface characteristics of TiO_2 and TiO_2/PAC at different calcination tempera-
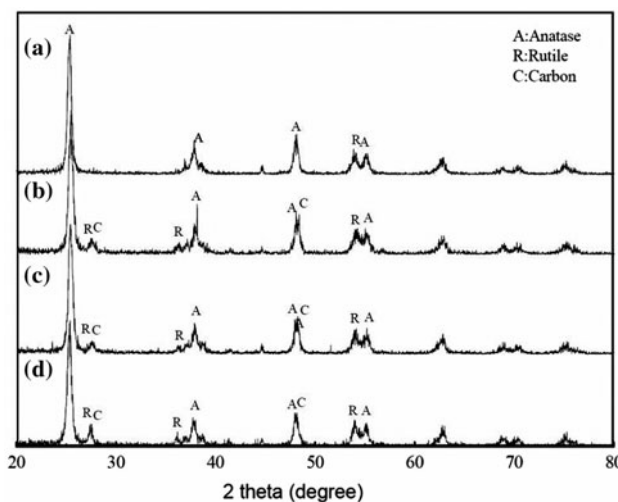
Fig. 2. XRD patterns of photocatalysts (a) TiO_2, (b) TiO_2/PAC (C/Ti = 0.2), (c) TiO_2/PAC (C/Ti = 0.5), and (d) TiO_2/PAC (C/Ti = 1) (calcination temp. = 400°C).

Table 1
Surface characteristics of TiO_2 and TiO_2/PAC (C/Ti = 1) at different calcination temperatures

Photocatalyst	Crystallination (%)		Particle size (nm)	BET (m^2/g)	Pore size (nm)	Pore volume (cm^3/g)
	Anatase	Rutile				
PAC	–	–	–	968	4	0.6395
TiO_2 (300℃)	62	38	40	47	9	0.1501
TiO_2 (400℃)	87	13	40	42	14	0.1814
TiO_2 (500℃)	49	51	49	38	23	0.2767
TiO_2/PAC (300℃)	88	12	26	163	11	0.1935
TiO_2/PAC (400℃)	91	9	28	108	17	0.1791
TiO_2/PAC (500℃)	90	10	49	27	20	0.1654

tures. The phases of the prepared TiO_2/PAC were mostly anatase with small amounts of rutile. Calcination at 400℃ generated the highest phase percentage of anatase in both TiO_2 and TiO_2/PAC. TiO_2 with the anatase crystalline structure typically exhibits higher photocatalytic activity than that with other crystalline structures, such as rutile and brookite. TiO_2 and TiO_2/PAC that are calcined at 400℃ may exhibit the highest photocatalytic activity.

Fig. 3. SEM micrographs of photocatalysts (a) TiO_2 and (b) TiO_2/PAC (calcination temp. = 400℃, C/Ti = 1).

The TiO_2/PAC crystals were smaller than the TiO_2 crystals (Table 1). Li et al. [22] made the same observation. The dispersion of TiO_2 on the surface of PAC inhibits aggregation of TiO_2 during calcination; hence, particle size reduced. Li et al. [22], Wang et al. [23], and Slimen et al. [13] also demonstrated that AC acts as a barrier that controls the growth of TiO_2 powder and prevents its agglomeration. Crystalline size increased with calcination temperature (Table 1); this trend resembles that identified by Li et al. [22] and Gao et al. [12]. The decrease in particle and pore sizes in TiO_2/PAC was correlated with the observed increase in surface area; additionally, surface area increased as pore volume increased (Table 1). The surface area of TiO_2/PAC increased by the doping the PAC surface on TiO_2 particles because PAC has a high surface area (300 and 400℃). The surface area of TiO_2 and TiO_2/PAC decreased as calcination temperature increased, in which the finding was similar to that of Wang et al. [10]. Adding PAC increased the surface area of the photocatalyst and reduced the size of the titania particles (Table 1).

Fig. 3 displays SEM micrographs of TiO_2 and TiO_2/PAC. The prepared TiO_2 and TiO_2/PAC mainly consisted of spherical nanoparticles with a high tendency to agglomerate and form a porous structure. The sizes of the aggregates of TiO_2 and TiO_2/PAC were approximately 40 and 30 nm, respectively (Fig. 3), agreeing with the values that were calculated from the XRD patterns (Table 1). Fig. 4 presents TEM images of TiO_2 and TiO_2/PAC. The TEM images indicate that the spherical nanoparticles agglomerated and they include crystal lattice lines.

XPS is a powerful technique for determining surface chemical composition. Fig. 5 presents the fitted XPS spectra of the C 1s region of TiO_2/PAC. The binding energies at 284.8 and 285.4 eV were attributed to
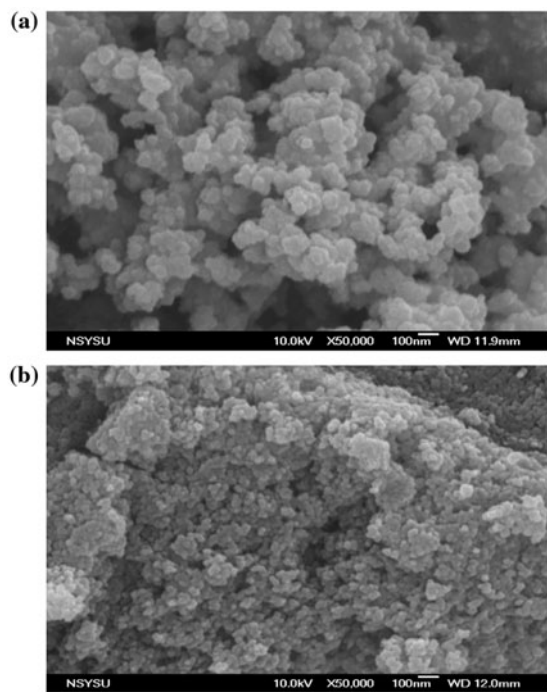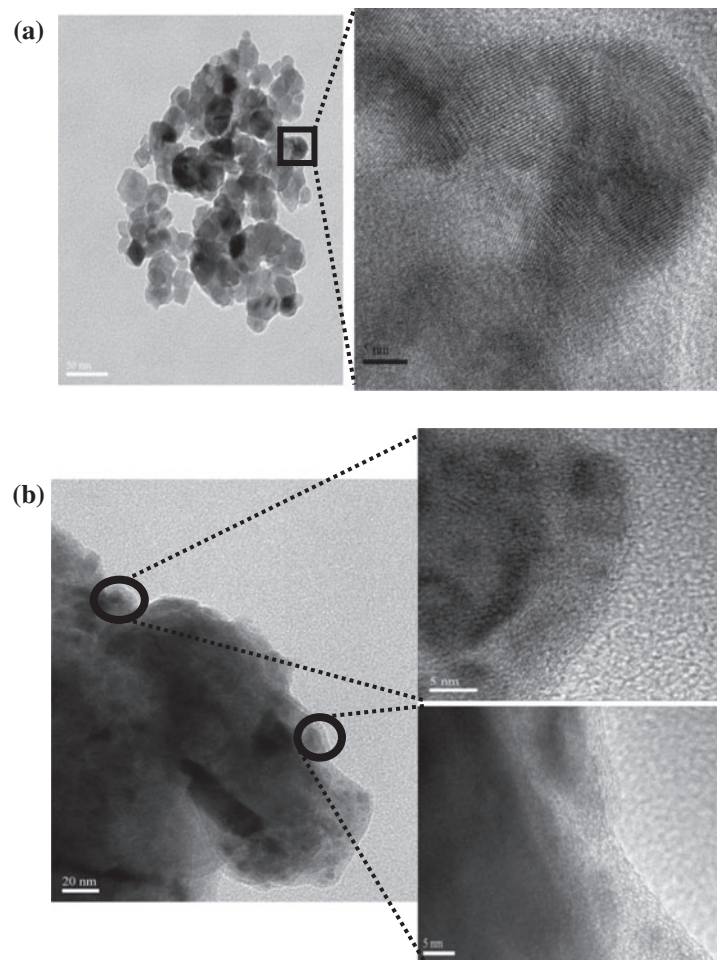
Fig. 4. TEM micrographs of photocatalysts (a) TiO$_2$ and (b) TiO$_2$/PAC (calcination temp. = 400 ℃, C/Ti = 1).
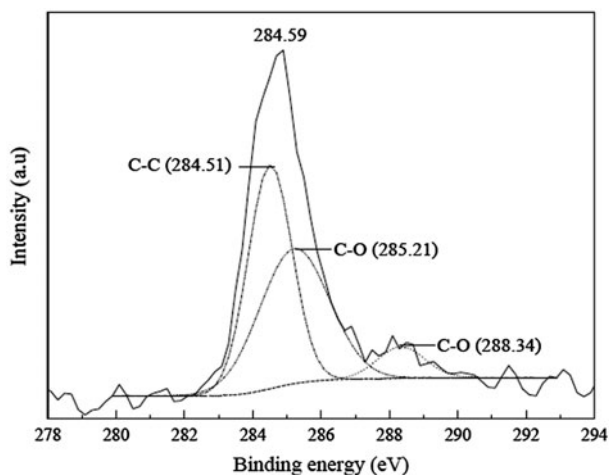
Fig. 5. Fitting XPS spectra for C 1s region of TiO$_2$/PAC (calcination temp. = 400 ℃, C/Ti = 1).

C–C and C–O bonds, respectively [14,21]. Kang et al. [17] demonstrated that the binding energy at 282 eV is attributable to the Ti–C bond that is formed by the substitution of carbon at the oxygen site in TiO$_2$; additionally, the binding energy at 288.6 eV is attributable to carbonate species following substitution of carbon at the Ti site in TiO$_2$. The prepared TiO$_2$/PAC included C–C and C–O bonds, but not Ti–C bonds. XPS analysis revealed that the ratio of C–C and C–O binding was 48 and 52% in TiO$_2$/PAC (C/Ti = 1), respectively; moreover, the C/Ti ratio was 0.87. The Ti 2p3/2 and Ti 2p1/2 spin-orbital splitting photoelectrons were located at binding energies 458.6 and 464.4 eV, which were assigned to Ti^{4+} (TiO$_2$) [24]. Based on the areas under the curves for Ti 2p (Fig. 6), the proportions of Ti 2p3/2 and Ti 2p1/2 in TiO$_2$ were 32 and 68%, respectively, and those in TiO$_2$/PAC were 34 and 66%, respectively. Peaks at 529.4 and 530.3 eV were assigned to O 1s; the former can be attributed to TiO$_2$ and the latter is attributable to absorbed hydroxyl groups [24]. Based on the O 1s calculation (Fig. 7), the number of absorbed hydroxyl groups on TiO$_2$/PAC (39%) exceeded that of those on TiO$_2$ (29%). When the TiO$_2$
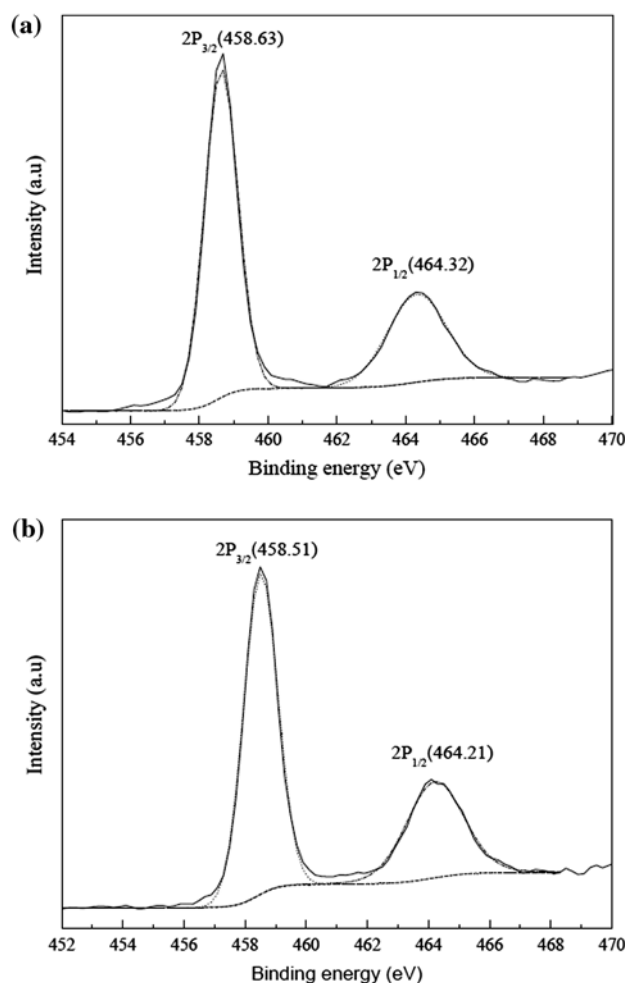
Fig. 6. XPS spectra for Ti 2p region (a) TiO$_2$ (b) TiO$_2$/PAC (calcination temp. = 400℃, C/Ti = 1).

Fig. 7. XPS spectra for O 1s region (a) TiO$_2$ (b) TiO$_2$/PAC (calcination temp. = 400℃, C/Ti = 1).

nanoparticles were deposited on PAC, the full width at half maximum (FWHM) values of the asymmetric bands at Ti 2p3/2 (from 1.2 to 1.3 eV) and Ti 2p1/2 (from 2.0 to 2.2 eV) increased (Fig. 6). Experimental results reveal that the bonds between TiO$_2$ and PAC were on the TiO$_2$/PAC interface. The FWHM of peaks from TiO$_2$/CNTs exhibited a similar trend [25]. XPS characterization confirms the substitution of O in the crystal lattice for C species in TiO$_2$/PAC, forming Ti–O–C (Figs. 5 and 7).

UV-vis diffuse reflectance spectra measurements revealed that the band gap of TiO$_2$/PAC at C/Ti = 0.2, 0.5, and 1 was 2.96, 2.94, and 2.63 eV, respectively; and the band gap of TiO$_2$ was 2.97 eV. The spectra indicate that the absorption edge of undoped TiO$_2$ (418 nm) shifted to a longer wavelength (471 nm) after C doping. The decrease in the band gap was attributed to the formation of Ti–O–C bonds [6]. As the PAC content increased, the strength of visible light absorption increased. A red shift indicates that the TiO$_2$/PAC was

excited to produce additional electron-hole pairs under light irradiation, potentially increasing photocatalytic activity. Numerous studies have also obtained a red shift in UV-vis diffuse reflectance spectra of TiO$_2$/carbon composites [5,6]. We suggest that PAC improves the thermal stability of titania by suppressing the anatase-to-rutile phase transformation and the growth of crystals (Table 1), and that it preserves a high number of surface hydroxyl groups (Fig. 7); these findings are similar to those of Wang et al. [23] and Slimen et al. [13].

3.2. Photodegradation efficiency in the TiO$_2$ and TiO$_2$/PAC systems

3.2.1. Effects of C/Ti ratio, calcination temperature, and the wavelength of the light source

Adsorption by the TiO$_2$ and the TiO$_2$/PAC (calcination temperature = 400℃) suspension and direct
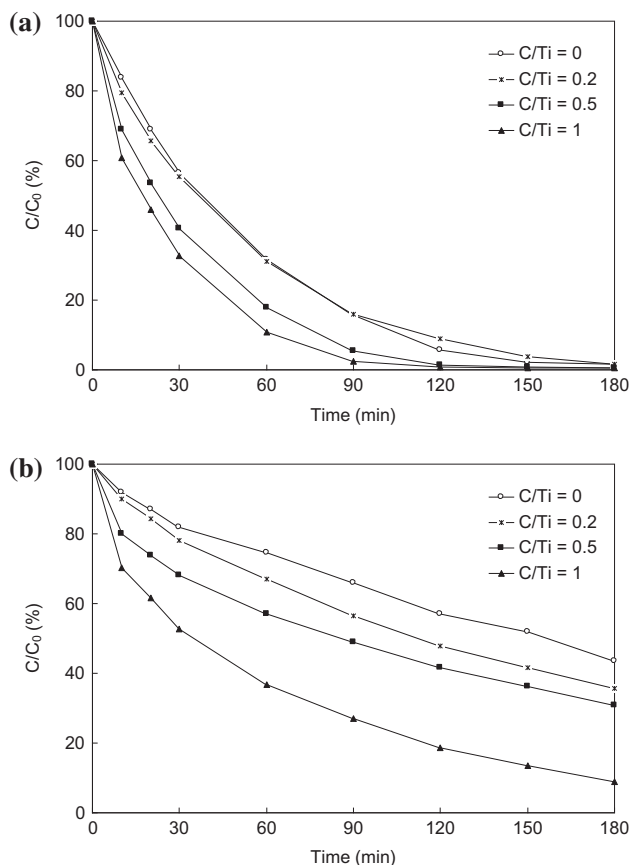
Fig. 8. Effects of C/Ti ratio on RR2 decolorization for UV/TiO₂/PAC (a) 254 nm (b) 365 nm ([RR2] = 20 mg/L, [photocatalyst] = 1 g/L, pH = 7, calcination temp. = 400°C).

photolysis of RR2 under 254, 365, and 410 nm irradiation were performed in background experiments to compare their efficiencies of decolorization, which are associated with photocatalytic reactions. At pH 7, the RR2 decolorization percentage achieved by 180 min of direct photolysis at 254, 365, and 410 nm irradiation was 14, 1, and 0.3%, respectively. When the dose of photocatalyst was 1 g/L, the RR2 decolorization achieved by the adsorption of TiO₂ and TiO₂/PAC during 180 min of reaction was 1.5 and 46%, respectively. Adsorption of RR2 by TiO₂/PAC was very high and we suggest that the high adsorption ability of TiO₂/PAC generates high photocatalytic efficiency for RR2 decolorization (discussed later). At a calcination temperature of 400°C, the effects of the C/Ti ratio of UV/TiO₂/PAC on RR2 decolorization were evaluated (Fig. 8). After 180 min of the reaction, the RR2 decolorization percentage achieved at C/Ti ratios of 0, 0.2, 0.5, and 1 in the UV (254 nm)/TiO₂/PAC system were 98, 99, 100, and 100%, respectively, and those in the UV (365 nm)/TiO₂/PAC system were 57, 64, 69, and 91%, respectively. Below 254 and 365 nm

irradiation, the decolorization efficiency of the TiO₂/PAC system increased with the C/Ti ratio. A high doping concentration of C increases the energy shift due to a large overlap of C and O states, leading to a narrow band gap in TiO₂/PAC, as obtained from band gap analysis results. Optimal amount of C, N, and/or S dopant exists, in which they synergistically serve as electron traps, inhibiting the recombination of photogenerated electron-hole pairs [26,27]. Excess dopant can serve as charge recombination centers;
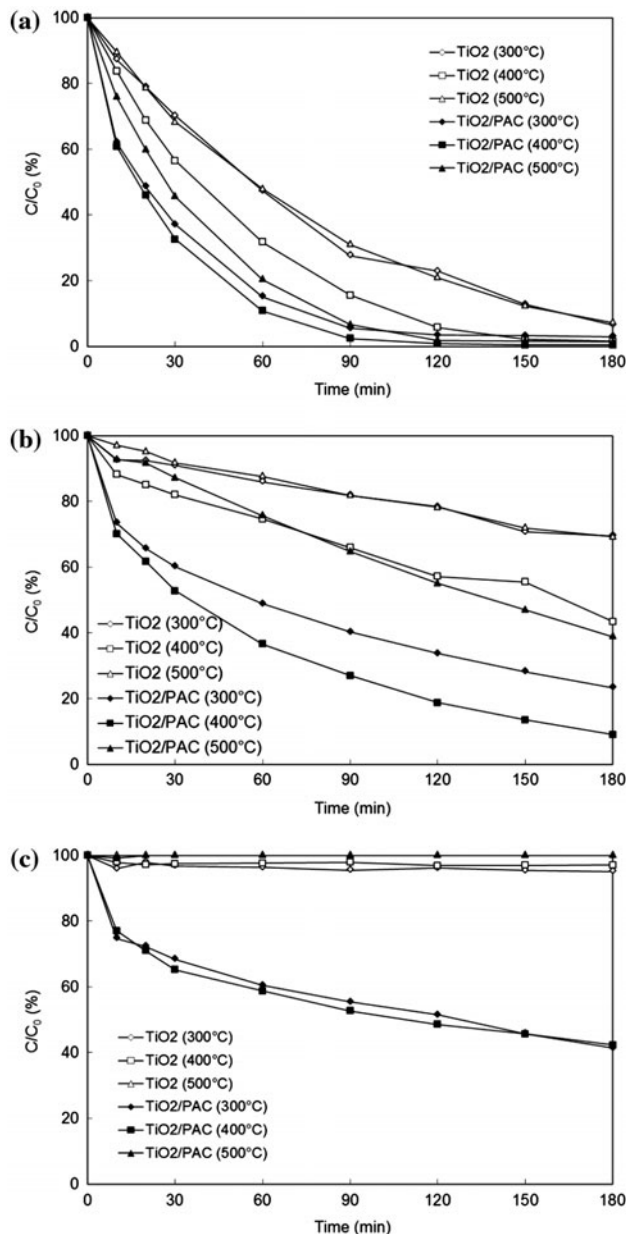
Fig. 9. Effects of calcination temperature on RR2 decolorization for TiO₂ and TiO₂/PAC systems (a) 254 nm (b) 365 nm (c) 410 nm ([RR2] = 20 mg/L, [photocatalyst] = 1 g/L, pH = 7, C/Ti = 1).

however, it was not observed to do so in TiO$_2$/PAC at C/Ti ratios of 0.2–1. Hence, TiO$_2$/PAC with a C/Ti ratio of one was selected as the photocatalyst in the following experiments.

Fig. 9 displays the effects of calcination temperature on RR2 decolorization using the TiO$_2$ and TiO$_2$/PAC systems under irradiation by light of different light wavelengths. After 180 min of reaction, the RR2 decolorization percentage at calcination temperatures of 300, 400, and 500°C in the UV (254 nm)/TiO$_2$/PAC system was 97, 100, and 99%, respectively; that in the UV (365 nm)/TiO$_2$/PAC system was 77, 91 and 61%, respectively, and that in the visible light (410 nm)/ TiO$_2$/PAC system was 59, 58, and 0%, respectively. The photocatalytic activity was highest at a calcination temperature of 400°C for both the TiO$_2$ and TiO$_2$/PAC systems; moreover, the photocatalytic activity of the TiO$_2$/PAC system exceeded that of the TiO$_2$ system. This distribution of TiO$_2$ on layers of PAC particles may cause charge transference between TiO$_2$ and PAC, improving the ability of photocatalysts to absorb light. Additionally, PAC acts as an electron acceptor that has an inductive effect, promoting the separation of photo-induced electron-hole pairs, retarding their recombination, and thereby increasing photocatalytic activity [8,9,11]. PAC functions as an effective adsorbent that concentrates pollutants around the loaded TiO$_2$, enhancing the pollutant transfer process, and thereby increasing photocatalytic efficiency [8,11,12]. This synergistic effect of TiO$_2$ and AC has been reported for the degradation of some organic compounds in the photocatalytic process [7–9,11–13].

Below 410 nm irradiation, only TiO$_2$/PAC that had been calcined at 300 or 400°C exhibited photocatalytic activities (Fig. 9(c)). Total PAC combustion occurs during calcination at over 400°C in the TiO$_2$/PAC system. In such a case herein, the surface area declined significantly at 500°C (Table 1), and the synergistic effect of the presence of a common contact interface between TiO$_2$ and PAC disappeared (Fig. 9(c)). The proportion of anatase phase in both the TiO$_2$ and TiO$_2$/PAC systems was great following calcination at 400°C. Accordingly, 400°C was selected as the optimal calcination temperature. After 150 min of the reaction under irradiation by 410 nm, the RR2 decolorization percentages that achieved using TiO$_2$/PAC (this work) and TiO$_2$/CNTs [15] were 55 and 60%, respectively. Kuo [15], who used TiO$_2$ and TiO$_2$/CNTs systems to decolorize RR2 under irradiation of various sources of light, found that the RR2 decolorization efficiency of both TiO$_2$ and TiO$_2$/CNTs systems followed the order 254 > 365 > 410 nm; moreover, the rate of decolorization achieved using TiO$_2$/CNTs exceeded than that achieved using TiO$_2$ under all light irradiation

Table 2
Effects of pH on RR2 decolorization rate constants for the TiO$_2$ and TiO$_2$/PAC systems ([RR2] = 20 mg/L, [photocatalyst] = 1 g/L, C/Ti = 1, calcination temp. = 400°C)

UV (nm)	254 nm		365 nm	
pH effects	k (hr^{-1})	R^2	k (hr^{-1})	R^2
TiO$_2$ (pH5)	1.26	0.988	0.40	0.737
TiO$_2$ (pH7)	1.20	0.997	0.27	0.957
TiO$_2$ (pH9)	0.66	0.984	0.17	0.997
TiO$_2$/PAC (pH5)	4.38	0.991	3.71	0.995
TiO$_2$/PAC (pH7)	2.41	0.997	0.83	0.964
TiO$_2$/PAC (pH9)	1.30	0.999	0.68	0.987

sources. The important findings of this study concerning TiO$_2$/PAC resemble those of Kuo for TiO$_2$/CNTs [15]. The TiO$_2$/PAC and TiO$_2$/CNTs systems were photoexcited under visible light irradiation. Although the role of PAC in the TiO$_2$/PAC system was similar to that of CNTs in the TiO$_2$/CNTs system, PAC is cheaper than CNTs. Hence, the TiO$_2$/PAC system is more suitable than the TiO$_2$/CNTs system for use in wastewater treatment.

3.2.2. Effects of pH, RR2 concentration, and photocatalyst dosage

The pH of solution significantly affected photodegradation. The pH influences the surface characteristics of a photocatalyst, the dissociation of RR2, and the formation of hydroxyl radicals. Table 2 lists the effects of pH on the RR2 decolorization rate constants (k) of the UV/TiO$_2$ and UV/TiO$_2$/PAC systems. The k values of RR2 in the UV/TiO$_2$ and UV/TiO$_2$/PAC systems fit pseudo-first-order kinetics, as has been reported in various studies of dye decolorization [28–30]. Low pH values do not support the production of hydroxyl groups and high pH values do not support the adsorption of RR2 on TiO$_2$ and/or TiO$_2$/PAC. Zhao et al. [31] demonstrated that the rates of dye adsorption and degradation were higher at lower pH because the alkaline medium retarded anion adsorption. Therefore, the decolorization rate constants in the UV/TiO$_2$ and UV/TiO$_2$/PAC systems followed the order pH 5 > pH 7 > pH 9 (Table 2).

In the UV/TiO$_2$ and UV/TiO$_2$/PAC systems, k values declined as the RR2 concentration increased (Table 3). This phenomenon existed for three possible reasons. First, as the initially RR2 concentration increased, increasing amounts of RR2 and reaction intermediates competed with both hydroxyl radicals

Table 3
Effects of RR2 concentration on RR2 decolorization rate constants for the TiO_2 and TiO_2/PAC systems ([photocatalyst] = 1 g/L, pH = 7, C/Ti = 1, calcination temp. = 400°C)

UV (nm)	254 nm		365 nm	
RR2 effects	k (hr^{-1})	R^2	k (hr^{-1})	R^2
TiO_2 (10 mg/L)	3.37	0.995	0.46	0.986
TiO_2 (20 mg/L)	1.20	0.997	0.27	0.957
TiO_2 (40 mg/L)	0.30	0.999	0.08	0.843
TiO_2/PAC (10 mg/L)	6.28	0.947	1.10	0.975
TiO_2/PAC (20 mg/L)	2.41	0.997	0.83	0.964
TiO_2/PAC (40 mg/L)	0.53	0.985	0.20	0.868

Table 4
Effects of photocatalyst dose on RR2 decolorization rate constants for the TiO_2 and TiO_2/PAC systems ([RR2] = 20 mg/L, pH = 7, C/Ti = 1, calcination temp. = 400°C)

UV (nm)	254 nm		365 nm	
Dose effects	k (hr^{-1})	R^2	k (hr^{-1})	R^2
TiO_2 (0.5 g/L)	1.06	0.993	0.13	0.963
TiO_2 (1 g/L)	1.20	0.997	0.17	0.969
TiO_2 (2 g/L)	1.55	0.994	0.32	0.963
TiO_2/PAC (0.5 g/L)	1.16	0.991	0.20	0.996
TiO_2/PAC (1 g/L)	2.41	0.997	0.83	0.964
TiO_2/PAC (2 g/L)	3.40	0.983	0.93	0.890

and active reaction sites on the photocatalyst surface. The rate of formation of hydroxyl radicals on the photocatalyst surface was constant because the amount of photocatalyst remained constant. Accordingly, the fraction of hydroxyl radicals that attack RR2 molecules and the reaction intermediates declined as the RR2 concentration increased. Second, a significant amount of UV light may be absorbed by highly concentrated RR2 molecules, rather than by photocatalyst particles, reducing decolorization efficiency. The dye thus has a UV-screening effect. Third, as the initial RR2 concentration increased, the photocatalyst surfaces adsorbed more RR2 molecules, inhibiting direct contact between RR2 molecules and photogenerated holes [32], and suppressing the formation of hydroxyl radicals on the photocatalyst surface because RR2 molecules covered active surface sites [1]. Many investigations have found similar results for the UV/TiO_2 system [1,29,32].

The RR2 decolorization rate increased as the photocatalyst dosage increased in the range 0.5–2 g/L (Table 4). Photogenerated holes and hydroxyl radicals were then produced, and the yields of the holes and radicals increased with the photocatalyst dosage. Therefore, the proportion of hydroxyl radicals that attacked RR2 and the reaction intermediates increased with the photocatalyst dosage. However, adding a large amount of photocatalyst may have reduced UV penetration and had a UV-screening effect, inhibiting photodegradation. This study found that the UV-screening effect of adding 2 g/L photocatalyst was negligible and was associated with the highest decolorization rate. After 1 g/L photocatalyst had been added and the reaction allowed to proceed for 240 min, the TOC removal percentage in the UV (254 nm)/TiO_2 and UV (254 nm)/TiO_2/PAC systems were 40 and 56%, respectively. The efficiencies of TiO_2/PAC in both decolorization and TOC removal were better than those of TiO_2.

4. Conclusions

In this work, TiO_2 and TiO_2/PAC are produced via the sol-gel method, and the prepared photocatalysts were applied to decolorize RR2 under irradiation by light of different wavelengths. The phases of prepared TiO_2/PAC were mainly anatase with a small amount of rutile. Adding PAC increased the surface area of the photocatalyst and reduced the size of titania particles. XPS characterization verified the substitution of C at the O sites in the crystal lattice in the TiO_2/PAC system, forming Ti–O–C. Additionally, the amount of hydroxyl groups that was adsorbed on TiO_2/PAC exceeded that on TiO_2. Under irradiation by light with a wavelength of 410 nm, only TiO_2/PAC that had been calcined at 300 or 400°C was photoexcited, and 400°C was found to be the optimal calcination temperature. The RR2 decolorization efficiency followed the order of 254 > 365 > 410 nm in both the TiO_2 and TiO_2/PAC systems. The RR2 decolorization rate increased as the pH and RR2 concentration decreased and as the photocatalyst dose increased. The PAC acted as an effective adsorbent and photo-induced electron acceptor; therefore, the photocatalytic efficiency of TiO_2/PAC exceeded that of TiO_2.

References

[1] I.K. Konstantinou, T.A. Albanis, TiO_2-assisted photocatalytic degradation of azo dyes in aqueous solution: Kinetic and mechanistic investigations—a review, Appl. Catal., B 49 (2004) 1–14.

[2] Y. Nakaoka, H. Katsumata, S. Kaneco, T. Suzuki, K. Ohta, Photocatalytic degradation of diazinon in aqueous solution by platinized TiO_2, Desalin. Water Treat. 13 (2010) 427–436.

[3] B. Ge, J. Zhang, P. Lei, X. Kong, Q. He, Study on degradation behavior of N, N-dimethylacetamide by photocatalytic oxidation in aqueous TiO_2 suspensions, Desalin. Water Treat. 42 (2012) 274–278.

[4] L. Mansouri, L. Bousselmi, Degradation of diethyl phthalate (DEP) in aqueous solution using TiO_2/UV process, Desalin. Water Treat. 40 (2012) 63–68.

[5] H. Wang, H.L. Wang, W.F. Jiang, Solar photocatalytic degradation of 2, 6-dinitro-p-cresol (DNPC) using multi-walled carbon nanotubes (MWCNTs)–TiO_2 composite photocatalysts, Chemosphere 75 (2009) 1105–1111.

[6] Y. Min, K. Zhang, W. Zhao, F. Zheng, Y. Chen, Y. Zhang, Enhanced chemical interaction between TiO_2 and grapheme oxide for photocatalytic decolorization of methylene bule, Chem. Eng. J. 193–194 (2012) 203–210.

[7] D.K. Lee, S.C. Kim, S.J. Kim, I.S. Chung, S.W. Kim, Photocatalytic oxidation of microcystin-LR with TiO_2-coated activated carbon, Chem. Eng. J. 102 (2004) 93–98.

[8] Y. Li, X. Li, J. Li, J. Yin, Photocatalytic degradation of methyl orange in a sparged tube reactor with TiO_2-coated activated carbon composites, Catal. Commun. 6 (2005) 650–655.

[9] Y. Li, X. Li, J. Li, J. Yin, Photocatalytic degradation of methyl orange by TiO_2-coated activated carbon and kinetic study, Water Res. 40 (2006) 1119–1126.

[10] W. Wang, C.G. Silva, J.L. Faria, Photocatalytic degradation of Chromotrope 2R using nanocrystalline TiO_2/activated-carbon composite catalysts, Appl. Catal., B 70 (2007) 470–478.

[11] C.C. Mao, H.S. Weng, Promoting effect of adding carbon black to TiO_2 for aqueous photocatalytic degradation of methyl orange, Chem. Eng. J. 155 (2009) 744–749.

[12] B. Gao, P.S. Yap, T.M. Lim, T.T. Lim, Adsorption-photocatalytic degradation of Acid Red 88 by supported TiO_2: Effect of activated carbon support and aqueous anions, Chem. Eng. J. 171 (2011) 1098–1107.

[13] H. Slimen, A. Houas, J.P. Nogier, Elaboration of stable anatase TiO_2 through activated carbon addition with high photocatalytic activity under visible light, J. Photochem. Photobiol., A 221 (2011) 13–21.

[14] G. An, W. Ma, Z. Sun, Z. Liu, B. Han, S. Miao, Z. Miao, K. Ding, Preparation of titania/carbon nanotube composites using supercritical ethanol and their photocatalytic activity for phenol degradation under visible light irradiation, Carbon 45 (2007) 1795–1801.

[15] C.Y. Kuo, Prevenient dye-degradation mechanisms using UV/TiO_2/carbon nanotubes process, J. Hazard. Mater. 163 (2009) 239–244.

[16] R.A. Spurr, H. Myers, Quantitative analysis of anatase-rutile mixtures with an X-Ray diffractometer, Anal. Chem. 29 (1957) 760–762.

[17] I.C. Kang, Q. Zhang, S. Yin, T. Sato, F. Saito, Preparation of a visible sensitive carbon doped TiO_2 photo-catalyst by grinding TiO_2 with ethanol and heating treatment, Appl. Catal., B 80 (2008) 81–87.

[18] J. Ovenstone, Preparation of novel titania photocatalysts with high activity, J. Mater. Sci. 36 (2001) 1325–1329.

[19] M. Toyoda, Y. Nanbu, Y. Nakazawa, M. Hirano, M. Inagaki, Effect of crystallinity of anatase on photoactivity for methyleneblue decomposition in water, Appl. Catal., B 49 (2004) 227–232.

[20] S.S. Arbuj, R.R. Hawaldar, U.P. Mulik, B.N. Wani, D.P. Amalnerkar, S.B. Waghmode, Preparation, characterization and photocatalytic activity of TiO_2 towards methylene blue degradation, Mater. Sci. Eng., B 168 (2010) 90–94.

[21] H.A. Le, L.T. Linh, S. Chin, J. Jurng, Photocatalytic degradation of methylene blue by a combination of TiO_2-anatase and coconut shell activated carbon, Powder Technol. 225 (2012) 167–175.

[22] Y. Li, S. Zhang, Q. Yu, W. Yin, The effects of activated carbon supports on the structure and properties of TiO_2 nanoparticles prepared by a sol–gel method, Appl. Surf. Sci. 253 (2007) 9254–9258.

[23] X. Wang, Z. Hu, Y. Chen, G. Zhao, Y. Liu, Z. Wen, A novel approach towards high performance composite photocatalyst of TiO_2 deposited on activated carbon, Appl. Surf. Sci. 255 (2009) 3953–3958.

[24] X. Zhang, M. Zhou, L. Lei, Preparation of an Ag–TiO_2 photocatalyst coated on activated carbon by MOCVD, Mater. Chem. Phys. 91 (2005) 73–79.

[25] L. Tian, L. Ye, K. Deng, L. Zan, TiO_2/carbon nanotube hybrid nanostructures: Solvothermal synthesis and their visible light photocatalytic activity, J. Solid State Chem. 184 (2011) 1465–1471.

[26] R. Asahi, T. Morikawa, T. Ohwaki, K. Aoki, Y. Taga, Visible-light photocatalysis in nitrogen-doped titanium oxides, Science 293 (2001) 269–271.

[27] J.A. Rengifo-Herrera, C. Pulgarin, Photocatalytic activity of N, S co-doped and N-doped commercial anatase TiO_2 powders towards phenol oxidation and *E. coli* inactivation under simulated solar light irradiation, Sol. Energy 84 (2010) 37–43.

[28] C. Lee, J. Yoon, Application of photoactivated periodate to the decolorization of reactive dye: Reaction parameters and mechanism, J. Photochem. Photobiol., A 165 (2004) 35–41.

[29] C.H. Wu, Effects of operational parameters on the decolorization of C.I. Reactive Red 198 in UV/TiO_2-based systems, Dyes Pigm. 77 (2008) 31–38.

[30] C.H. Wu, Photodegradation of C.I. Reactive Red 2 in UV/TiO_2-based systems: Effects of ultrasound irradiation, J. Hazard. Mater. 167 (2009) 434–439.

[31] J. Zhao, T. Wu, K. Wu, K. Oikawa, H. Hidaka, N. Serpone, Photoassisted degradation of dye pollutants. 3. Degradation of the cationic dye rhodamine B in aqueous anionic surfactant/TiO_2 dispersions under visible light irradiation: Evidence for the need of substrate adsorption on TiO_2 particles, Environ. Sci. Technol. 32 (1998) 2394–2400.

[32] N. Daneshvar, D. Salari, A.R. Khataee, Photocatalytic degradation of azo dye Acid Red 14 in water: Investigation of the effect of operational parameters, J. Photochem. Photobiol., A 157 (2003) 111–116.